Noninvasive Visualization of RNA Delivery with ^{99m}Tc-Radiolabeled Small-Interference RNA in Tumor Xenografts

Lei Kang[1], Rong Fu Wang[1], Ping Yan[1], Meng Liu[1], Chun Li Zhang[1], Ming Ming Yu[1], Yong Gang Cui[1], and Xiao Jie Xu[2]

[1]*Department of Nuclear Medicine, Peking University First Hospital, Beijing, China; and* [2]*Institute of Biotechnology, Academy of Military Medical Sciences, Beijing, China*

Small-interference RNAs (siRNAs) are short, double-strand RNA molecules that target specific messenger RNAs for degradation via the process termed RNA interference. The efficacy of RNA interference depends greatly on effective delivery of siRNA, which calls for noninvasive methods for tracing siRNA in vivo. The purpose of this work was to develop a novel ^{99m}Tc-radiolabeled method to visualize siRNA targeting of a tumor biomarker of human telomerase reverse transcriptase (hTERT) in HepG2 tumor xenografts. **Methods:** After conjugation with *S*-acetyl *N*-hydroxysuccinimide-mercaptoacetyltriglycine (NHS-MAG3), antisense RNA with 2′-*O*-methyl modification was annealed with sense strand to form a duplex and then radiolabeled with ^{99m}Tc. ^{99m}Tc-siRNAs were tested for stability in serum by measurement of radiochemical purity and for inhibitory activity by reverse-transcriptase polymerase chain reaction and Western blotting. In vitro cellular uptake was evaluated in HepG2 cells. Biodistribution studies and static imaging were performed in HepG2 tumor–bearing mice. **Results:** Radiochemical purity remained highly stable in saline and fresh human serum at room temperature and 37°C. Radiolabeled siRNA demonstrated strong inhibitory effects similar to those of unlabeled siRNA on both hTERT messenger RNA and protein in vitro. ^{99m}Tc-hTERT siRNA showed more uptake than did control siRNA in HepG2 cells after 1 h of incubation. After administration in HepG2 tumor–bearing mice, ^{99m}Tc-hTERT siRNA had significantly higher accumulation in tumors and a higher tumor-to-blood ratio than did control siRNA ($P < 0.05$). Scintigraphy of ^{99m}Tc-hTERT siRNA showed clear tumor images at 0.5, 1, 3, and 6 h after injection. In contrast, ^{99m}Tc-control siRNA failed to visualize the tumor. Ratios of uptake in tumor to uptake in contralateral region of hTERT-targeted siRNA were significantly higher than those of control siRNA ($P < 0.05$) at each time point. **Conclusion:** The ^{99m}Tc radiolabeling method with NHS-MAG3 chelator can be used successfully in siRNA radiolabeling, allowing for the noninvasive visualization of siRNA delivery in vivo.

Key Words: ^{99m}Tc; small-interference RNA (siRNA); delivery; human telomerase reverse transcriptase (hTERT); molecular imaging

J Nucl Med 2010; 51:978–986
DOI: 10.2967/jnumed.109.069906

Received Aug. 27, 2009; revision accepted Feb. 16, 2010.
For correspondence or reprints contact: Rong Fu Wang, Department of Nuclear Medicine, Peking University First Hospital, No. 8, Xishiku St., Xicheng West District, Beijing, 100034, China.
E-mail: rongfu_wang2003@yahoo.com.cn

RNA interference (RNAi) technology has been considered one of the most outstanding and powerful tools in gene therapy research (*1*). In the process of RNAi, a kind of short, double-strand RNA molecule called small-interference RNA (siRNA) targets specific messenger RNAs (mRNAs) for degradation. The discovery of siRNAs has gained great attention in the development of gene therapy. However, when siRNA is used as RNAi therapeutics in vivo, many problems have arisen, such as off-target effect, low bioactivity, and limited delivery (*2*). The efficacy of RNAi in vivo depends greatly on the effective delivery of siRNA. Therefore, a noninvasive, convenient, and inexpensive technique for tracing the delivery of siRNA in vivo is required. Although some optical imaging techniques such as fluorescence and bioluminescence have been used (*3,4*), they are limited at the level of cell culture and small-animal model because of insufficient emitting energy and low resolution (*5*). Compared with these optical methods, radionuclide tracing methods have great advantages such as high sensitivity, quantitative determination, availability in large animals, and promising clinical application (*6*). When radiolabeled with γ- or positron-emitting isotopes, siRNA is able to show its location, quantity, and duration by noninvasive imaging (*7*). Moreover, radiolabeled with γ- and β-emitting isotopes such as ^{131}I, siRNA probes can achieve the dual effect of imaging and therapy.

In a previous study of radionuclide imaging of ^{99m}Tc-labeled RNA (*8*), only sense or antisense single-strand RNA was described, instead of duplex RNA. Therefore, no conclusion about distribution of duplex siRNA was drawn. Superior to single-strand RNA, duplex RNA has more stability and a longer half-life in serum (*9*). Numerous hydrogen bonds between double strands provide thermal stability and protection against nucleases. Furthermore, it was reported that duplex formation could improve delivery in cell culture, probably because of more lipophilic exposure leading to better capability of diffusing across cell membranes (*10*). On the basis of these studies, duplex siRNA should be considered for noninvasive imaging in vivo.

However, one challenge for siRNA-based imaging is the instability of siRNA in radiolabeling and biologic systems. Fortunately, some effective methods of chemical modification have been developed to improve RNA thermal stability and resistance against nuclease digestion, such as phosphorothioate linkages (*11*) and 2′-position modification in ribose (*12*). Compared with phosphorothioate linkages, 2′-*O*-methyl (2′-OMe) sugar modification occurs naturally in mammalian ribosomal RNA and transfer RNA and is, thus, nontoxic to cells. In addition to improving nuclease resistance of internucleotide phosphate bonds, 2′-OMe can also decrease the likelihood of triggering immune response, lower the incidence of off-target effect, and improve pharmacodynamics (*13*). Therefore, this intrinsic modification makes siRNA stable in radiolabeling and biologic systems.

Human telomerase reverse transcriptase (hTERT) is highly expressed in different kinds of human cancers (>85%) but undetectable in most normal cells (*14*). This distinction allows hTERT to be an important biomarker of malignant tumors, leading to high expectation for hTERT as a visualized (*15*) or therapeutic target (*16*). In a previous study, we successfully showed the visualization of hTERT expression by ^{99m}Tc-radiolabled antisense oligonucleotide and proved hTERT mRNA as an attractive candidate for antisense imaging (*17*). In this study, we described the preparation and preclinical studies of a ^{99m}Tc-radiolabeled duplex siRNA that targeted hTERT. The aim of this study was to develop a new noninvasive method to visualize the delivery of siRNA in vivo and provide a potential siRNA-based imaging method.

MATERIALS AND METHODS

siRNA

hTERT-targeted siRNA was against the sequence of 5′-TTTCATCAGCAAGTTTGGA-3′ on the 14th exon of hTERT mRNA, according to its significant inhibitory effect in a previous study (*18*). Control siRNA was against the sequence of 5′-TTCTCCGAACGTGTCACGT-3′, which targeted none of the human genes. Both sense and antisense RNAs were synthesized with uniform 2′-OMe modification by GenePharma Corp. Because a duplex will dissociate as soon as it recognizes its target, *N*-hydroxysuccinimide-mercaptoacetyltriglycine (NHS-MAG3) should be conjugated with an antisense (guide) strand instead of a sense (passenger) strand. Otherwise, the sense strand labeled with ^{99m}Tc will depart from the target into cytoplasm, resulting in the decrease of sensitivity and specificity of imaging. Therefore, a primary amine was added at the 5′ end of antisense RNA via a 6-carbon methylene linker to conjugate with the bifunctional chelator for ^{99m}Tc labeling. At the 3′ end of each single strand, a deoxythymidine overhang was added to increase the stability and binding efficiency. Chemical synthesized RNAs were purified and analyzed with high-performance liquid chromatography. Lyophilized RNAs were stored at −80°C. All solvents were prepared with diethylpyrocarbonate-treated water.

Mercaptoacetyltriglycine RNA Conjugation and RNA Annealing

NHS-MAG3 was selected as the bifunctional chelator because of its high radiolabeling efficiency under gentle reaction conditions of ambient temperature and neutral pH (*19*). NHS-MAG3 was generously provided by Yi Wang (University of Massachusetts Medical School). Mercaptoacetyltriglycine was chelated with RNA as described previously for oligonucleotide (*20,21*). In brief, lyophilized RNA was dissolved in 0.30 M *N*-2-hydroxyethylpiperazine-*N*-2-ethanesulfonic acid buffer at a concentration of 10 μg/μL, pH 8.0. A fresh 20 mg/mL solution of NHS-MAG3 in anhydrous *N,N*-dimethylformamide was added, dropwise with soft agitation, to a final mercaptoacetyltriglycine-to-RNA molar ratio of 20:1. After incubation at room temperature for 1–2 h, conjugated products were purified with a 0.7 × 28 cm Sephadex G25 (GE Amersham) column, using 0.25 M ammonium acetate as eluant. Peak fractions were pooled according to the RNA absorbance at 260 nm measured by NanoDrop 1000 (Thermo Scientific). Then RNA products were dispensed at 10 μg per tube and lyophilized with a centrifugal evaporator (SpeedVac).

After the molecular weight (MW) analysis of conjugated RNA by AXIMA-CFRplus (Kratos), sense and antisense RNAs were hybridized (*22*). Equal amounts of complementary strands were mixed in annealing buffer (50 mM NaCl, 10 mM dithiothreitol, 10 mM $MgCl_2$, and 10 mM Tris-Cl, pH 7.5) at a concentration of 1 μg/μL. The mixture was heated at 90°C for 1 min and then incubated at 37°C for 1 h. Hybridized duplexes were lyophilized and stored at −80°C.

Radiolabeling with ^{99m}Tc

Both hTERT-targeted and control siRNA duplexes were radiolabeled with ^{99m}Tc in the same way. Briefly, 50 mg/mL of sodium tartrate solution was prepared with 0.5 M sodium bicarbonate, 0.25 M ammonium acetate, and 0.175 M ammonium hydroxide, pH 9.2. The solution was added into a 0.25 M ammonium acetate buffer (pH 5.2) containing a 500 μg/mL concentration of mercaptoacetyltriglycine–RNA to a final concentration of 7 μg/μL. $SnCl_2{\cdot}2H_2O$ solution (1 mg/mL) was prepared with a 100 mg/mL solution of sodium tartrate buffer. Then, 1 μL of fresh $SnCl_2{\cdot}2H_2O$ was added immediately after 37–74 MBq of fresh ^{99m}Tc-pertecnetate in 10–20 μL were added. Radiolabeled products were purified on a 0.7 × 28 cm Sephadex G25 column with 0.25 M ammonium acetate as eluant. Radioactivity and absorbance of all fractions at 260 nm were analyzed.

Double-phase paper chromatography on filter paper (no. 1; Xinhua) was performed to measure labeling efficiency and radiochemical purity, with acetone and normal saline as mobile phases (*17*).

Serum Stability

^{99m}Tc-siRNA probes were incubated in saline or fresh human serum at room temperature and 37°C, respectively, at a concentration of 0.01 μg/μL. In vitro stability was evaluated by measuring radiochemical purities at 0.5, 1, 2, 3, 4 and 6 h.

Cell Culture and Transfection

Hepatocarcinoma HepG2 cells from the American Type Culture Collection were cultured in Dulbecco's modified Eagle's medium (Invitrogen) supplemented with 10% fetal bovine serum (Invitrogen), 100 units of penicillin per milliliter, and 100 μg of streptomycin per milliliter under a 5% CO_2 atmosphere at 37°C. Adherent cells were transfected as described by the manufacturer. In transfection, cells always reached 80% confluence and were maintained in medium without antibiotics.

Inhibitory Activity Studies

Cells were cultured in 6-well plates with 5×10^5 cells in each well. The mixture containing 100 pmol of RNA and 5 μL of liposome (Lipofectamine 2000; Invitrogen) in 500 μL of serum-reduced Opti-MEM (Invitrogen) was added to each well. Then cells were incubated with transfection mixture for 6 h and further cultured for 48–72 h for reverse-transcriptase polymerase chain reaction (RT-PCR) and Western blotting analysis. For mock experiments, cells were treated under the same conditions without siRNA.

For RT-PCR, cells were washed twice with phosphate-buffered saline (PBS) (Invitrogen) followed by total RNA extraction by Trizol (Invitrogen). First-strand cDNA was synthesized with random primers and Moloney murine leukemia virus reverse transcriptase (YPH Bio). Polymerase chain reaction primers for hTERT were 5′-CGGAAGAGTGTCTGGAGCAA3′ and 5′-GGATGAAGCGGAGTCTGGA (*23*), and those for glyceraldehyde-3-phosphate dehydrogenase were 5′-CATCAAGAAGGTGGTGAAGC-3′ and 5′-ACCCTGTTGCTGTAGCCAA-3′. Amplification was performed with DNA polymerase (CHIMERx), with an initial heating at 95°C for 5 min; 35 cycles of 95°C, 60°C, and 72°C for 30 s, respectively; and finally an extension for 10 min at 72°C. Polymerase chain reaction products were analyzed by 2% agarose (Biowest) gel electrophoresis and visualized with an ultraviolet transilluminator (α-Innotech).

For Western blotting, cells were lysed with the solution containing 50 mM Tris-HCl (pH 7.4), 150 mM NaCl, 1% NP-40, 0.1% sodium dodecyl sulfate, and 10% Proteinase Inhibitor Cocktail Set I (Roche). Proteins (200 μg) were subjected to 8% sodium dodecyl sulfate polyacrylamide gel electrophoresis, transferred onto a polyvinylidene difluoride membrane (Millipore), and immunoblotted with rabbit anti-TERT polyclonal antibody (1:500; Santa Cruz). The membrane was also blotted with anti-β-tubulin antibody (Santa Cruz) as control. After incubation with horseradish peroxidase–labeled goat antirabbit IgG (Amersham), the membrane was visualized by Chemiluminescence Luminant Reagent (Santa Cruz) and exposed to ECL Hyperfilm (Kodak) for 3–20 min.

Cellular Uptake Kinetics

In vitro cellular uptake was analyzed in 24-well plates with 1×10^5 HepG2 cells per well and evaluated under 2 conditions: with or without transfection. For transfection, a mixture containing 1 pmol of ^{99m}Tc-siRNAs and 1 μL of liposome in 100 μL of Opti-MEM was added into each well. For nontransfection, 1 pmol of ^{99m}Tc-siRNA in 100 μL of Opti-MEM was added directly into the medium. Cells were incubated at 37°C and harvested at 10 min, 30 min, 1 h, 2 h, 4 h, and 6 h. Each well was rinsed with PBS 3 times. Counts containing radioactive medium and PBS were defined as C_{out}. After being lysed with 0.5 M sodium hydroxide and 1% sodium dodecyl sulfate, cells were washed 3 times. Radioactivity counts of lysis solution and PBS were defined as C_{in}. Cellular uptake ratio was calculated by the formula $C_{in}/(C_{in} + C_{out})$.

Animal Model

All animal studies conformed to the requirements of the Institutional Animal Care and Use Committee of Peking University. BALB/c *nu/nu* mice (female; weight ± SD, 20 ± 4 g; age, 4–6 wk) were kept in the Department of Laboratory Animal Science (Peking University Health Science Center). HepG2 cells (1×10^7; hTERT-positive expression) were injected subcutaneously in the right upper armpit of each mouse. When tumors reached a diameter of 1.0 cm, HepG2 tumor–bearing mice were administered hTERT-targeted and control ^{99m}Tc-siRNAs.

Biodistribution

Each mouse was injected with 1 μg (1,850 kBq) of ^{99m}Tc-siRNAs in 200 μL of saline via the tail vein. At 0.5, 1, 2, 4, and 6 h, 5 mice were sacrificed by cervical dislocation after 100 μL of blood samples were collected. Tissues of interest (heart, liver, spleen, lung, kidney, stomach, small intestine, bladder, skeletal muscle, bone marrow, and tumor) were removed and weighed. Radioactivity of all tissues was measured with a NaI (Tl) well counter. Biodistribution results were recorded as percentage of injected dose per gram (%ID/g).

SPECT

^{99m}Tc-siRNAs (4 μg [7.4 MBq]) in 200 μL of saline were injected via the tail vein. At 0.5, 1, 3, and 6 h, mice were laid on a face-up detector and imaged by a SPECT scanner (SPR SPECT; GE Healthcare) equipped with a low-energy, high-resolution, parallel-hole collimator. Static anterior images, collecting 200,000 counts, were stored as a 256×256 matrix at 2.0 zoom. The ratio of radioactive counts in the tumor to that in the contralateral equivalent region was calculated by drawing regions of interest at each time point.

Statistical Analysis

Variables are expressed as average ± SD. Statistical comparisons of variables were performed by ANOVA analysis. *P* values of less than 0.05 were considered statistically significant.

RESULTS

Conjugation

The mercaptoacetyltriglycine group was chelated with RNA via the primary amine, whereas protecting groups of NHS ester and *S*-acetyl were removed (Supplemental Fig. 1 supplemental materials are available online only at http://jnm.snmjournals.org). Matrix-assisted laser desorption/ionization time-of-flight mass spectroscopy analysis showed that the MW of the antisense strand before conjugation was 7,061.4 (Fig. 1A), and the MW after conjugation was 7,307.1 (Fig. 1B). The increased MW of 245.7 correlated with the MW of the mercaptoacetyltriglycine group (245.23).

Radiolabeling

Under the optimal conditions of a reaction time of 1 h and the addition of 1 μg/μL of $SnCl_2 \cdot 2H_2O$, average labeling efficiency reached 73.4% ± 3.0% ($n = 5$) at room temperature. After purification with Sephadex G25, the specific activity was up to 25.9 Gbq/μmol, and the radiochemical purity was no less than 92%. With the mobile phase of acetone, ^{99m}Tc-RNA and colloids remained at the bottom (Rf = 0–0.1), and ^{99m}Tc-pertechnetate moved to the top (Rf = 0.9–1). With the mobile phase of saline, ^{99m}Tc-siRNA (Rf = 0.8–1) and ^{99m}Tc-pertechnetate (Rf = 0.9–1) migrated with the solvent, and colloids remained at the origin (Rf = 0–0.1). In contrast, the labeling efficiency of siRNA without chelating mercaptoacetyltriglycine was

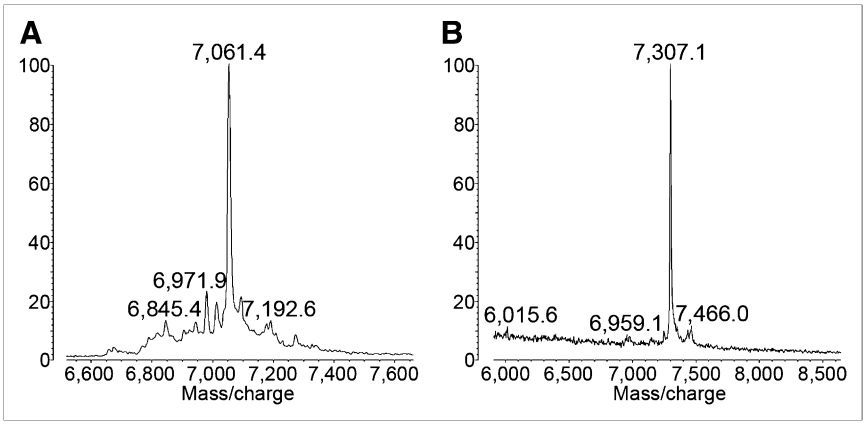

FIGURE 1. Matrix-assisted laser desorption/ionization time-of-flight mass spectroscopy analysis of antisense RNA before (A) and after (B) chelation with mercaptoacetyltriglycine.

3.0% ± 1.3% (n = 5), indicating that the radiolabeling of siRNA with ^{99m}Tc was mediated with mercaptoacetyltriglycine chelator.

Serum Stability

The radiochemical purity of ^{99m}Tc-hTERT siRNA was more than 94% and highly stable in 6 h. Radiolabeled siRNA exhibited no significant degradation and off-labeling. No significant trend for the radiochemical purity to be lower in fresh human serum than in saline was observed in the incubation (Fig. 2). It was shown that radiolabeled siRNA had a good tolerance in serum at 37°C, which was similar to the condition in vivo.

In Vitro Inhibitory Activity of ^{99m}Tc-hTERT siRNA

After transfection, RT-PCR and Western blotting were performed to evaluate the inhibitory activity of ^{99m}Tc-hTERT siRNA on hTERT mRNA and protein. Compared with cells untreated or transfected with liposome, cells transfected with siRNAs showed a significant decrease of hTERT mRNA ($P < 0.05$). A similar inhibitory effect of mRNA was observed in both unlabeled siRNA (81.33% ± 1.22%) and labeled siRNA (79.21% ± 1.64%). Western blotting also showed a knocking-down effect of siRNAs on hTERT protein, with the average inhibitory rate of 76.68%, in contrast to the expression of housekeeping protein β-tubulin (Fig. 3). No significant difference in protein inhibition between unlabeled siRNA (76.32% ± 3.43%) and labeled siRNA (76.78% ± 2.95%) was seen. Inhibitory activity studies indicated that mercaptoacetyltriglycine conjugation and ^{99m}Tc radiolabeling did not affect the biologic activity of siRNA.

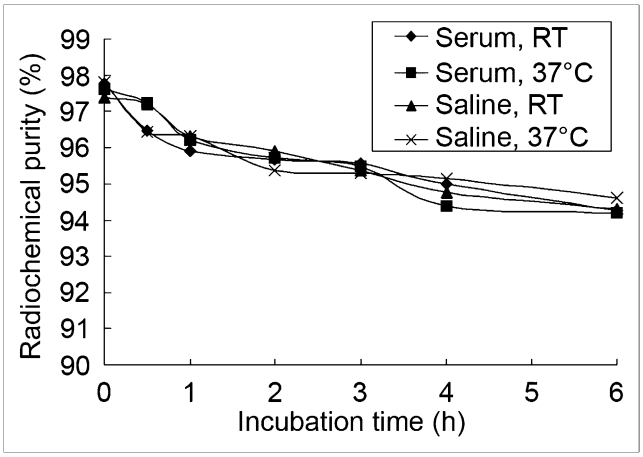

FIGURE 2. Radiochemical purity of ^{99m}Tc-hTERT siRNA in saline and fresh serum during 6 h, at room temperature (RT) and 37°C. Concentration of radiolabeled siRNA was 0.01 μg/μL.

In Vitro Cellular Uptake

Cellular uptake of both hTERT-targeted and control siRNAs increased gradually in the 6-h incubation (Fig. 4). Cellular uptake of both siRNAs with transfection was higher than the cellular uptake without transfection at same time point. With transfection, the uptake of hTERT siRNA was 2.19% ± 0.13%, 2.52% ± 1.24%, and 4.37% ± 0.52% at 10 min, 30 min, and 1 h, respectively, and the uptake of control siRNA was 2.42% ± 0.41%, 3.27% ± 0.08%, and 4.35% ± 0.04% at the same times. The similar uptake between both siRNAs in 1-h incubation suggested nonspecific transference through the cell membrane. After 1 h, the cellular uptake of ^{99m}Tc-hTERT siRNA increased faster than the uptake of control siRNA. A significant difference of cellular uptake between hTERT siRNA and control siRNA under the same condition from 2 to 6 h ($P < 0.05$) was observed. At 6 h, the cellular uptake of ^{99m}Tc-hTERT siRNA with or without transfection reached its maximum of 50.22% ± 1.90% or 32.86% ± 1.46% (n = 4), respectively, whereas the uptake of ^{99m}Tc-control siRNA reached a maximum of only 24.71% ± 1.04% or 20.57% ± 1.76% (n = 4).

Biodistribution Study

Biodistribution results (%ID/g) of ^{99m}Tc-hTERT siRNA and ^{99m}Tc-control siRNA are listed in Tables 1 and 2. For each siRNA, radioactive accumulation was found primarily in the kidneys and then in the liver. The radioactivity in blood decreased rapidly after injection. Blood-rich tissues such as the heart, lung, spleen, and bone marrow had

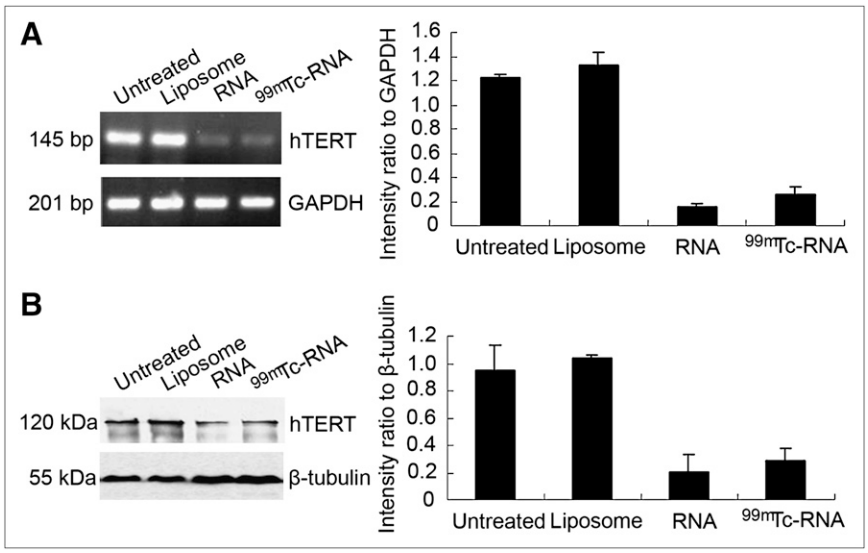

FIGURE 3. Inhibitory effect of hTERT-targeted siRNA on mRNA (A) and protein expression (B) by RT-PCR and Western blotting. HepG2 cells untreated, transfected with liposome, transfected with unlabeled siRNA, and transfected with labeled siRNA were analyzed. GAPDH = glyceraldehyde-3-phosphate dehydrogenase.

radioactivity accumulations similar to blood. The radioactivity in the gastrointestinal system was not high.

The radioactivity of ^{99m}Tc-hTERT siRNA in tumors increased from 0.82 ± 0.16 %ID/g to 0.97 ± 0.15 %ID/g from 1 to 6 h, but radioactivity in other tissues gradually decreased. In contrast, the radioactivity of ^{99m}Tc-control siRNA in tumors decreased from 1.88 ± 0.05 %ID/g to 0.16 ± 0.06 %ID/g, and radioactivity in other tissues also decreased gradually. There was a significant difference in tumor accumulation ($P < 0.05$) between hTERT-targeted and control siRNA. The increased tumor accumulation of hTERT-targeted siRNA might be related to the specific targeting instead of nonspecific accumulation. This result was confirmed by the comparison of tumor-to-nontumor (T/NT) ratios between ^{99m}Tc-hTERT siRNA and ^{99m}Tc-control siRNA (Figs. 5A and 5B). Except for the liver, lung, intestine, and muscle, there were significant differences in T/NT ratios in other tissues in the 6 h-incubation between these 2 probes ($P < 0.05$). At 6 h, T/NT ratios of hTERT-targeted siRNA were significantly higher than those of control siRNA in all tissues ($P < 0.05$). Ratios of tumor to blood and tumor to muscle for ^{99m}Tc-hTERT siRNA increased gradually and reached 2.62 ± 0.70 and 6.02 ± 0.52 ($n = 5$), respectively, at 6 h. However, the tumor-to-blood ratio of ^{99m}Tc-control siRNA rarely exceeded 1.00.

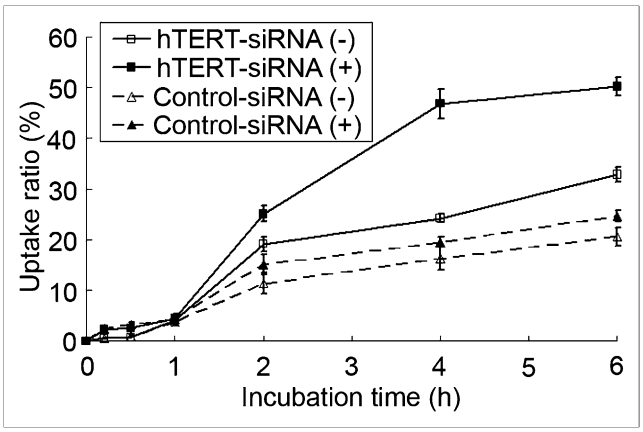

FIGURE 4. In vitro cellular uptake kinetics of ^{99m}Tc-radiolabeled hTERT-targeted and control siRNAs at 10 min, 30 min, 1 h, 2 h, 4 h, and 6 h. + = treatment with transfection; − = treatment without transfection.

γ-Camera Scintigraphy

Static images were obtained at 0.5, 1, 3, and 6 h after the administration of ^{99m}Tc-radiolabeled siRNAs. As predicted from the biodistribution study, primary radioactivity accumulation was found in the abdominal region. After the administration of ^{99m}Tc-hTERT siRNA, the intensity of radioactivity in the whole body decreased gradually. The tumor was clearly visualized shortly after injection and was shown most clearly at 6 h. hTERT-targeted siRNA indicated the specific accumulation in tumors and the slower clearance in tumors than in other tissues (Fig. 6A). Moreover, ratios of radioactive counts in tumors to those in the contralateral equivalent nontumor region increased gradually and were 2.68 ± 0.21, 2.92 ± 0.31, 4.96 ± 0.44, and 5.86 ± 0.30 at 0.5, 1, 3, and 6 h, respectively. In contrast, no tumor was clearly imaged during the 6 h after the administration of ^{99m}Tc-control siRNA (Fig. 6B). Tumor–to–contralateral nontumor ratios of control siRNA decreased from 0.5 to 6 h and were 1.55 ± 0.16, 1.39 ± 0.11, 1.31 ± 0.14, and 1.28 ± 0.12 at 0.5, 1, 3, and 6 h, respectively (Fig. 6C). The tumor–to–contralateral nontumor ratio of hTERT-targeted siRNA was significantly higher than that of control siRNA at each time point ($P <$ 0.05).

DISCUSSION

The successful application of siRNA in the laboratory has led to a high expectation for siRNA as a therapeutic

TABLE 1. Biodistribution (%ID/g) of ^{99m}Tc-hTERT siRNA in Tumor-Bearing Mice

Tissue	0.5 h	1 h	2 h	4 h	6 h
Heart	0.76 ± 0.10	0.43 ± 0.05	0.41 ± 0.14	0.38 ± 0.10	0.32 ± 0.06
Liver	7.68 ± 0.84	3.08 ± 0.32	1.63 ± 0.38	1.56 ± 0.12	0.99 ± 0.05
Spleen	0.78 ± 0.15	0.50 ± 0.11	0.41 ± 0.07	0.36 ± 0.05	0.25 ± 0.08
Lung	1.36 ± 0.09	1.03 ± 0.23	0.98 ± 0.10	0.96 ± 0.08	0.65 ± 0.15
Kidney	9.31 ± 2.68	5.80 ± 2.80	4.47 ± 0.85	2.72 ± 0.63	1.99 ± 0.59
Stomach	3.06 ± 0.84	1.66 ± 0.10	1.44 ± 0.40	1.24 ± 0.27	1.20 ± 0.35
Small intestine	4.20 ± 1.93	2.77 ± 0.76	2.10 ± 1.24	0.95 ± 0.41	0.64 ± 0.07
Bladder	2.60 ± 0.78	2.08 ± 0.33	2.39 ± 0.41	3.42 ± 2.30	3.56 ± 0.49
Skeletal muscle	0.61 ± 0.15	0.31 ± 0.04	0.58 ± 0.49	0.22 ± 0.05	0.17 ± 0.01
Bone marrow	1.06 ± 0.21	0.59 ± 0.06	0.39 ± 0.19	0.19 ± 0.05	0.10 ± 0.03
Blood	0.88 ± 0.14	0.52 ± 0.03	0.44 ± 0.06	0.43 ± 0.08	0.40 ± 0.06
Tumor	1.08 ± 0.07	0.82 ± 0.16	0.71 ± 0.14	0.74 ± 0.15	0.97 ± 0.15

Each value represents average of 5 mice ± SD.

agent. The delivery of siRNA in vivo is important to the identification of targeted tissues and evaluation of interference effect. In this study, the ^{99m}Tc radiolabeling method with NHS-MAG3 chelator was first used for siRNA. This method has been considered available for DNA radiolabeling; however, whether it can be applied to RNA is still unknown when the instability and nuclease degradation of RNA is taken into account. This purpose of this study was to evaluate the feasibility of noninvasively tracing the delivery of siRNA by ^{99m}Tc radiolabeling.

Some radiolabeling methods have been reported for tracing delivery of siRNA. Although siRNA can be labeled with ^{3}H using heat exchange (*24*) or labeled with ^{32}P using 5′-phosphorylation (*25*), these methods cannot noninvasively visualize the delivery of siRNA. Chelated with DOTA or diethylenetriaminepentaacetic acid, siRNA can be labeled with ^{111}In or ^{64}Cu and thus be visualized (*26,27*). Unfortunately, cyclotron production of ^{64}Cu and ^{111}In limits their wide application. ^{99m}Tc was selected in this study because of its proper emitting energy (140.5 keV), ready preparation, and safe use in basic and clinical fields (*6*). Before RNA is labeled with ^{99m}Tc, it needs to be chelated with NHS-MAG3, which provides coordinate groups for labeling. In contrast to low labeling efficiency without mercaptoacetyltriglycine conjugation (3%), the labeling efficiency with conjugation (76%) indicated the importance of the chelator NHS-MAG3. Moreover, the lack of a significant influence on the efficacy of siRNA after labeling showed that this radiolabeling method did not affect siRNA activity. This finding can probably be attributed to the low MW and simple structure of mercaptoacetyltriglycine (*28*). Compared with other RNA radiolabeling methods using diethylenetriaminepentaacetic acid (*27*), DOTA (*26*), or hydrazinonicotinamide (*8*), this NHS-MAG3 radiolabeling method provided a superior specific activity of 25.9 GBq/μmol. Furthermore, by means of chelation with NHS-MAG3, other siRNA probes carrying amine linkers could also be radiolabeled with ^{99m}Tc. Therefore, this radiolabeling method seems not only suitable for hTERT siRNA in this study but also promising for other siRNA labeling in potential preclinical and clinical studies.

In this study, uniform 2′-OMe modification was performed to protect siRNA from harsh physical and chemical conditions and nuclease degradation. During the incubation,

TABLE 2. Biodistribution (%ID/g) of ^{99m}Tc-control-siRNA in Tumor-Bearing Mice

Tissue	0.5 h	1 h	2 h	4 h	6 h
Heart	0.68 ± 0.37	0.34 ± 0.09	0.27 ± 0.07	0.16 ± 0.02	0.18 ± 0.05
Liver	4.22 ± 0.94	2.20 ± 0.92	1.27 ± 0.32	0.88 ± 0.12	0.49 ± 0.15
Spleen	1.68 ± 0.66	0.51 ± 0.23	0.38 ± 0.12	0.27 ± 0.04	0.13 ± 0.08
Lung	1.13 ± 0.44	0.76 ± 0.10	0.48 ± 0.13	0.23 ± 0.08	0.22 ± 0.04
Kidney	10.17 ± 3.86	8.20 ± 1.61	5.74 ± 1.90	2.14 ± 0.86	1.85 ± 0.58
Stomach	0.87 ± 0.35	2.21 ± 0.72	1.41 ± 0.50	0.86 ± 0.24	0.52 ± 0.21
Small intestine	1.66 ± 0.72	0.80 ± 0.05	0.41 ± 0.13	0.25 ± 0.04	0.23 ± 0.02
Bladder	2.83 ± 0.78	1.77 ± 0.76	0.32 ± 0.09	0.22 ± 0.11	0.28 ± 0.17
Skeletal muscle	1.18 ± 0.36	0.31 ± 0.07	0.21 ± 0.08	0.11 ± 0.04	0.08 ± 0.02
Bone marrow	1.01 ± 0.71	0.35 ± 0.03	0.24 ± 0.04	0.19 ± 0.00	0.14 ± 0.05
Blood	2.55 ± 0.81	0.93 ± 0.36	0.56 ± 0.17	0.33 ± 0.02	0.33 ± 0.14
Tumor	1.88 ± 0.05	0.66 ± 0.19	0.43 ± 0.09	0.27 ± 0.04	0.16 ± 0.06

Each value represents average of 5 mice ± SD.

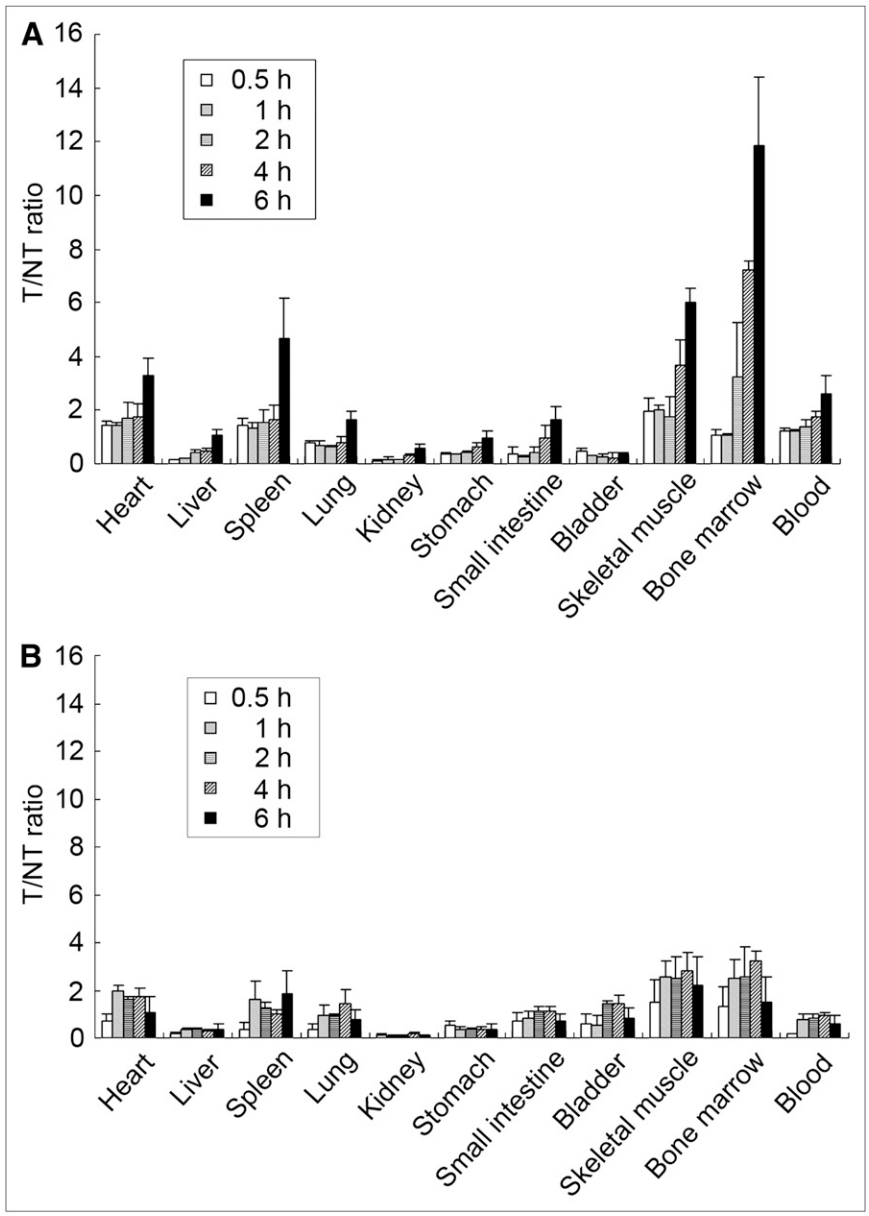

FIGURE 5. T/NT ratios of different tissues in nude mice bearing HepG2 tumor xenografts at 0.5, 1, 2, 4, and 6 h after injection of ^{99m}Tc-hTERT siRNA (A) and ^{99m}Tc-control siRNA (B). T/NT ratios were calculated from data in Tables 1 and 2.

2′-OMe-modified siRNA maintained high radiochemical purity in serum and inhibitory effect after conjugation, radiolabeling, and purification. Moreover, increasing accumulation of hTERT siRNA in the tumors proved the targeting ability of modified siRNA in vivo. Unfortunately, full 2′-OMe modification has been reported to suppress or dramatically decrease RNAi activity (*29*). However, some other studies showed siRNAs with full 2′-OMe modification could maintain interference efficacy (*22,30*). The tolerance of this modification is not confirmed but probably relates to probe design, duplex unwinding, RNA-induced silencing complex loading, and such (*22*). Full 2′-OMe modification indeed provides effective protection for siRNAs in vivo while avoiding immune response and toxicity.

To prove this, siRNA imaging was based on specific targeting of siRNA rather than the nonspecific delivery of unlabeled free ^{99m}Tc, and cellular uptake, biodistribution, and imaging between hTERT-targeted and control siRNAs were compared. In transfection, liposome envelops RNA probes so that lipophilic siRNA can easily pass through cell membranes. But this transference is nonspecific and bidirectional. In this study, cellular uptake of both probes was similar before 1 h and was nonspecific. After 1 h, more and more siRNAs were transfected into cells so that cellular uptakes of both siRNAs increased. However, hTERT siRNA could target mRNA specifically, thus staying in cells, whereas control siRNA did not bind to any target so it moved freely at the same time. The differential cellular uptake of hTERT-targeted and control siRNA presented their specific and nonspecific delivery in HepG2 cells. The average in vitro cellular uptake of ^{99m}Tc-siRNA (30%) was higher than that of ^{99m}Tc-labeled antisense DNA (15%)

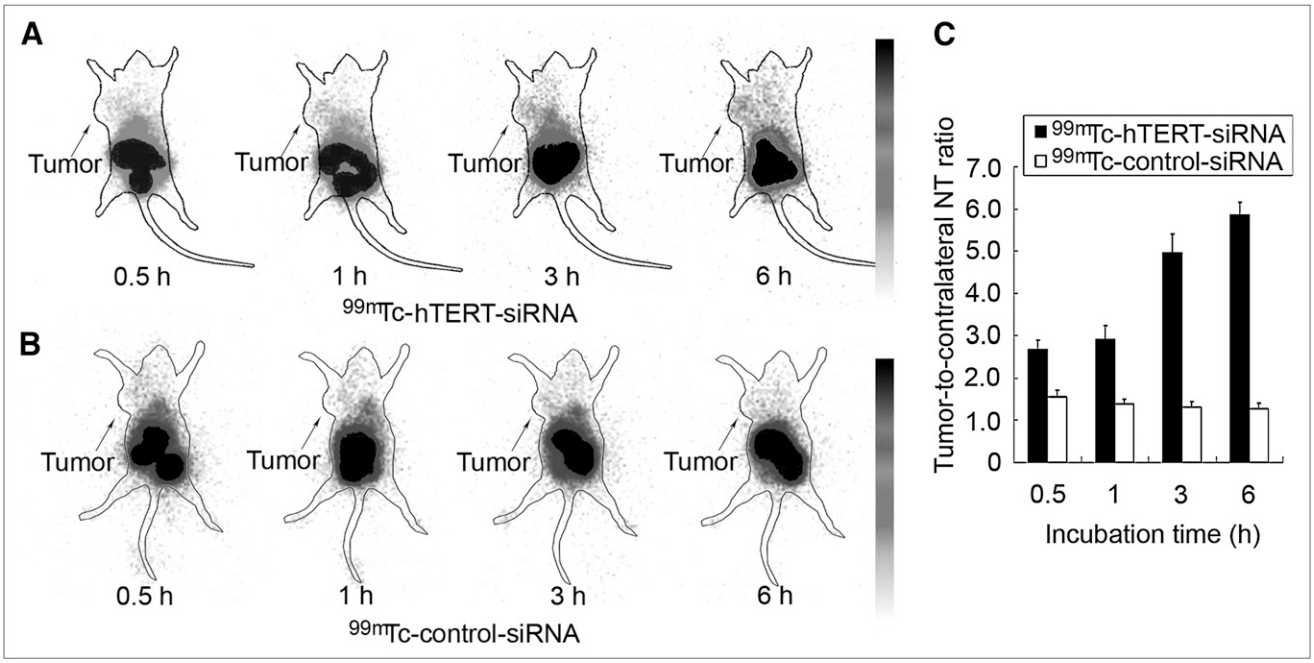

FIGURE 6. γ-camera scintigraphy of nude mice bearing HepG2 tumor xenografts at 0.5, 1, 3, and 6 h after administration of ^{99m}Tc-hTERT siRNA (A) and ^{99m}Tc-control siRNA (B). Comparison of tumor–to–contralateral nontumor ratios (C) showed significant difference between the 2 siRNAs ($P < 0.05$). Arrows indicate tumor placement. NT = nontumor.

(*17*) or that of single-strand RNA (12%) (*8*). This result suggested that a duplex could improve cellular delivery, which may be related to the better diffusing capability of duplex (*10*), different targets, and different cell types. Although liposomes could improve the delivery of siRNA in vitro, the usage of liposome in vivo was seriously limited by its potential toxicity, disordered tumor vessel, and extensive tumor stroma (*3*). Moreover, the increase of tumor accumulation and tumor-to-blood ratio of ^{99m}Tc-hTERT siRNA proved the successful transporting of the naked siRNA to the hTERT mRNA in vivo. In contrast to control siRNA, ^{99m}Tc-hTERT siRNA showed significantly higher tumor accumulation in vivo, indicating that in vivo images represented the specific delivery of ^{99m}Tc-labeled siRNA. Therefore, ^{99m}Tc-hTERT siRNA may be used for visualizing the hTERT mRNA in the tumor.

If applied in siRNA-based imaging, ^{99m}Tc-hTERT siRNA seemed to encounter the same problem of high-radioactivity accumulation in the kidneys and liver as other nucleotide probes, such as antisense DNA (*17*), naked siRNA (*31*), and siRNA nanoparticles (*26*). High accumulation in the kidneys and liver could be explained by strong reabsorption by proximal tubules (*31*) and phosphorothioate scavenging by endothelial cells in the liver (*32*). High accumulation in normal tissues might cause potential toxicity. However, hTERT is not expressed in most normal tissue, and the accumulation of hTERT siRNA in the kidneys and liver is nonspecific. siRNA won't play its inhibiting role in these tissues; thus, the potential toxicity should be tiny. Moreover, the acute toxicity of antisense probes with similar accumulation in small animals has not yet been found (*33*). Another disadvantage of high accumulation in the abdomen is that collected radioactivity counts in tumor are relatively decreased in static imaging, resulting in poor tumor images. An antifolate pemetrexed was applied to reduce renal uptake in radiofolate imaging and improved radioactivity collection in tumors (*34*). However, whether it can be used in siRNA imaging is still unknown.

CONCLUSION

The ^{99m}Tc radiolabeling method with NHS-MAG3 chelator can be successfully used in siRNA radiolabeling. Furthermore, ^{99m}Tc-MAG3-siRNA provides a prospective approach for the noninvasive imaging of the delivery of siRNA in vivo; thus this method can be potentially applied in the straightforward and quantitative evaluation of the RNAi effect in vivo.

ACKNOWLEDGMENTS

We thank Yi Wang (current affiliation, University of Massachusetts Medical School) for the generous gift of NHS-MAG3 and Fengqing Guo (Peking University First Hospital) for animal injection. This study was supported by grants from the National Natural Science Foundation of China (NSFC 30670583, 30870729, and 30900374), National Basic Research Program (973 Program, 2006CB705705-1), second phase of National Education Ministry 985 Project (985-2-056), Key Laboratory of Radiopharmaceuticals

Program from Ministry of Education of China (0706), and Research Fund for the Doctoral Program of Higher Education of China (200800011061).

REFERENCES

1. Elbashir SM, Harborth J, Lendeckel W, Yalcin A, Weber K, Tuschl T. Duplexes of 21-nucleotide RNAs mediate RNA interference in cultured mammalian cells. *Nature.* 2001;411:494–498.
2. Akhtar S, Benter I. Toxicogenomics of non-viral drug delivery systems for RNAi: potential impact on siRNA-mediated gene silencing activity and specificity. *Adv Drug Deliv Rev.* 2007;59:164–182.
3. Medarova Z, Pham W, Farrar C, Petkova V, Moore A. In vivo imaging of siRNA delivery and silencing in tumors. *Nat Med.* 2007;13:372–377.
4. Santangelo PJ, Lifland AW, Curt P, et al. Single molecule-sensitive probes for imaging RNA in live cells. *Nat Methods.* 2009;6:347–349.
5. Mocanu JD, Yip KW, Skliarenko J, et al. Imaging and modulating antisense microdistribution in solid human xenograft tumor models. *Clin Cancer Res.* 2007;13:5935–5941.
6. Hnatowich DJ. Antisense and nuclear medicine. *J Nucl Med.* 1999;40:693–703.
7. Bogdanov AA Jr. Merging molecular imaging and RNA interference: early experience in live animals. *J Cell Biochem.* 2008;104:1113–1123.
8. Liu N, Ding H, Vanderheyden JL, Zhu Z, Zhang Y. Radiolabeling small RNA with technetium-99m for visualizing cellular delivery and mouse biodistribution. *Nucl Med Biol.* 2007;34:399–404.
9. Braasch DA, Jensen S, Liu Y, et al. RNA interference in mammalian cells by chemically-modified RNA. *Biochemistry.* 2003;42:7967–7975.
10. Liu X, Nakamura K, Wang Y, et al. Improved delivery in cell culture of radiolabeled antisense DNAs by duplex formation. *Mol Imaging Biol.* 2006;8: 278–283.
11. Eckstein F. Phosphorothioate oligodeoxynucleotides: what is their origin and what is unique about them? *Antisense Nucleic Acid Drug Dev.* 2000;10:117–121.
12. Grünweller A, Wyszko E, Bieber B, Jahnel R, Erdmann VA, Kurreck J. Comparison of different antisense strategies in mammalian cells using locked nucleic acids, 2′-*O*-methyl RNA, phosphorothioates and small interfering RNA. *Nucleic Acids Res.* 2003;31:3185–3193.
13. Takahashi M, Minakawa N, Matsuda A. Synthesis and characterization of 2′-modified-4′-thioRNA: a comprehensive comparison of nuclease stability. *Nucleic Acids Res.* 2009;37:1353–1362.
14. Kim NW, Piatyszek MA, Prowse KR, et al. Specific association of human telomerase activity with immortal cells and cancer. *Science.* 1994;266:2011–2015.
15. Padmanabhan P, Otero J, Ray P, et al. Visualization of telomerase reverse transcriptase (hTERT) promoter activity using a trimodality fusion reporter construct. *J Nucl Med.* 2006;47:270–277.
16. Kim SH, Chung HK, Kang JH, et al. Tumor-targeted radionuclide imaging and therapy based on human sodium iodide symporter gene driven by a modified telomerase reverse transcriptase promoter. *Hum Gene Ther.* 2008;19:951–957.
17. Liu M, Wang RF, Zhang CL, et al. Noninvasive imaging of human telomerase reverse transcriptase (hTERT) messenger RNA with ^{99m}Tc-radiolabeled antisense probes in malignant tumors. *J Nucl Med.* 2007;48:2028–2036.
18. Masutomi K, Yu EY, Khurts S, et al. Telomerase maintains telomere structure in normal human cells. *Cell.* 2003;114:241–253.
19. Hnatowich DJ, Chang F, Lei K, Qu T, Rusckowski M. The influence of temperature and alkaline pH on the labeling of free and conjugated MAG_3 with technetium-99m. *Appl Radiat Isot.* 1997;48:587–594.
20. Wang Y, Liu G, Hnatowich DJ. Methods for MAG_3 conjugation and ^{99m}Tc radiolabeling of biomolecules. *Nat Protoc.* 2006;1:1477–1480.
21. Liu G, Zhang S, He J, Zhu Z, Rusckowski M, Hnatowich DJ. Improving the labeling of *S*-acetyl NHS-MAG_3-conjugated morpholino oligomers. *Bioconjug Chem.* 2002;13:893–897.
22. Kraynack BA, Baker BF. Small interfering RNAs containing full 2′-*O*-methylribonucleotide-modified sense strands display Argonaute2/eIF2C2-dependent activity. *RNA.* 2006;12:163–176.
23. Nakamura TM, Morin GB, Chapman KB, et al. Telomerase catalytic subunit homologs from fission yeast and human. *Science.* 1997;277:955–959.
24. Mook OR, Baas F, de Wissel MB, Fluiter K. Evaluation of locked nucleic acid-modified small interfering RNA in vitro and in vivo. *Mol Cancer Ther.* 2007;6: 833–843.
25. Wolfrum C, Shi S, Jayaprakash KN, et al. Mechanisms and optimization of in vivo delivery of lipophilic siRNAs. *Nat Biotechnol.* 2007;25:1149–1157.
26. Bartlett DW, Su H, Hildebrandt IJ, Weber WA, Davis ME. Impact of tumor-specific targeting on the biodistribution and efficacy of siRNA nanoparticles measured by multimodality in vivo imaging. *Proc Natl Acad Sci USA.* 2007;104: 15549–15554.
27. Merkel OM, Librizzi D, Pfestroff A, Schurrat T, Béhé M, Kissel T. In vivo SPECT and real-time γ camera imaging of biodistribution and pharmacokinetics of siRNA delivery using an optimized radiolabeling and purification procedure. *Bioconjug Chem.* 2009;20:174–182.
28. Zhang YM, Liu N, Zhu ZH, Rusckowski M, Hnatowich DJ. Influences of different chelators (HYNIC, MAG_3 and DTPA) on tumor cell accumulation and mouse biodistribution of technetium-99m labeled to antisense DNA. *Eur J Nucl Med.* 2000;27:1700–1707.
29. Chiu YL, Rana TM. siRNA function in RNAi: a chemical modification analysis. *RNA.* 2003;9:1034–1048.
30. Bramsen JB, Laursen MB, Nielsen AF, et al. A large-scale chemical modification screen identifies design rules to generate siRNAs with high activity, high stability and low toxicity. *Nucleic Acids Res.* 2009;37:2867–2881.
31. van de Water FM, Boerman OC, Wouterse AC, Peters JG, Russel FG, Masereeuw R. Intravenously administered short interfering RNA accumulates in the kidney and selectively suppresses gene function in renal proximal tubules. *Drug Metab Dispos.* 2006;34:1393–1397.
32. Park SY, Kwak W, Thapa N, et al. Combination therapy and noninvasive imaging with a dual therapeutic vector expressing MDR1 short hairpin RNA and a sodium iodide symporter. *J Nucl Med.* 2008;49:1480–1488.
33. Wang RF, Liu M, Zhang CL, et al. Study on pharmacokinetics and acute toxicity of ^{99m}Tc-radiolabeled antisense probes targeting human telomerase reverse transcriptase (hTERT) mRNA [abstract]. *J Nucl Med.* 2008;49(suppl 1):315–316.
34. Müller C, Forrer F, Schibli R, Krenning EP, de Jong M. SPECT study of folate receptor-positive malignant and normal tissues in mice using a novel ^{99m}Tc-radiofolate. *J Nucl Med.* 2008;49:310–317.